Two-level Electrochemical-model-based Estimation of Li-ion Battery State of Charge - Real-data Validation on an Electric Vehicle Use Case

Iulian Munteanu, Antoneta Iuliana Bratcu, Gildas Besancon, Didier Georges, Pierre-Xavier Thivel, Yann Bultel

▶ **To cite this version:**

Iulian Munteanu, Antoneta Iuliana Bratcu, Gildas Besancon, Didier Georges, Pierre-Xavier Thivel, et al.. Two-level Electrochemical-model-based Estimation of Li-ion Battery State of Charge - Real-data Validation on an Electric Vehicle Use Case. CCTA 2024 - 8th IEEE Conference on Control Technology and Applications, Aug 2024, Newcastle Upon Tyne, United Kingdom. hal-04652010

HAL Id: hal-04652010
https://hal.science/hal-04652010

Submitted on 17 Jul 2024

HAL is a multi-disciplinary open access archive for the deposit and dissemination of scientific research documents, whether they are published or not. The documents may come from teaching and research institutions in France or abroad, or from public or private research centers.

L'archive ouverte pluridisciplinaire **HAL**, est destinée au dépôt et à la diffusion de documents scientifiques de niveau recherche, publiés ou non, émanant des établissements d'enseignement et de recherche français ou étrangers, des laboratoires publics ou privés.

Two-level Electrochemical-model-based Estimation of Li-ion Battery State of Charge – Real-data Validation on an Electric Vehicle Use Case

Iulian MUNTEANU, Antoneta Iuliana BRATCU, Gildas BESANÇON, Didier GEORGES
Univ. Grenoble Alpes, CNRS, Grenoble INP, GIPSA-lab, 38000 Grenoble, France*
Institute of Engineering and Management Univ. Grenoble Alpes
{iulian.munteanu,antoneta.bratcu,gildas.besancon,didier.georges}@grenoble-inp.fr

Pierre-Xavier THIVEL, Yann BULTEL
Univ. Grenoble Alpes, Univ. Savoie Mont Blanc, CNRS, Grenoble INP, LEPMI, 38000 Grenoble, France*
Institute of Engineering and Management Univ. Grenoble Alpes
pierre-xavier.thivel@univ-grenoble-alpes.fr, yann.bultel@grenoble-inp.fr

***Abstract*—This paper proposes a two-level hierarchical estimation structure of a lithium-ion battery state of charge (SoC) based on the parabolic-partial-differential-equation Single Particle Model (SPM). Using a suitable linear finite-dimensional approximation of this model, it is proposed that the SoC estimation to be done in two dynamically-separated levels, consistent with the multi-time-scale nature of battery internal phenomena: a fast level implementing a dynamic inversion, in charge of retrieving surface concentrations of lithium based on output voltage measures, and a slow level, in which internal lithium concentrations are estimated by employing a Luenberger observer. After having first suitably calibrated the model, this structure is easy to tune and allows avoiding estimation convergence issues frequently occurring in the case of a global, one-level estimation and which are partly due to a numerically ill conditioned linear approximated model. SoC estimation accuracy is validated by using real data issued from battery cycling in an electric vehicular application, that is, under standard driving cycle scenarios. Estimation errors – computed against Coulomb counting taken as baseline estimation of battery SoC – are smaller than 3.5%, thus suggesting very satisfactory performance.**

***Index Terms*—battery electrochemical model, Single Particle Model (SPM), state of charge (SoC) estimation, state observer, dynamic inversion**

I. Introduction

Lithium-ion batteries are ubiquitous in electrical vehicle (EV) applications, having superior performance in key characteristics such as energy-to-weight ratio, output current, discharge capability, and total number of discharge cycles. Their successful and riskless use is done *via* Battery Management Systems (BMS) and supposes real-time knowledge of battery states. The lack of real-time internal measurements and the complexity of cell internal electrochemical phenomena – which renders difficult battery modeling and parameter identification – lead to significant inaccuracies in battery state of charge (SoC) estimators that are used in practical BMS [1]. That is why the search of advanced cell SoC estimators is a richly investigated research topic [2]– [5], often relying on complex physics-based electrochemical models, like Single Particle Model (SPM) [1], rather than on insufficiently representative equivalent electrical circuit models.

A lot of research effort has been dedicated to render these estimators efficient in practical applications. For example, in order to obtain very small SoC estimation errors, (Extended) Kalman filters have been used, [2], or else direct PDE observer design [6]. More recently, nonlinear observers based on a finite-dimensional approximation of SPM have been proposed, as well as improvements by the so-called hybrid multi-observer redesign [7], [8]. Also, including electrolyte behavior and temperature variation in the model, leading to the so-called Extended SPM [9], is a way to enhance estimation accuracy. However, these complex approaches come with a significant computational burden, which should be avoided in automotive applications. Moreover, the efficiency of these observers is hindered by improper model parameter identification, a topic richly addressed in the literature [10], [11]. Various simplifications – of either the model or the associated parameters – have thus been proposed [6], [12], [13].

In the same spirit, of using sufficiently simplified approach, within a pragmatic, engineering practice viewpoint, this paper proposes a SoC observer structure in which the estimation of interest variables is done in two dynamically-separated levels. The cell model complexity is maintained at a minimum, while retaining the phenomena essential to the battery cell electrochemical behavior captured by the SPM.

The paper is organized as follows. Section II is focused on battery cell modeling and Section III details the proposed SoC observer design and convergence. Section IV presents observer validation results both in simulation and by using real data relevant to EV use cases. Section V concludes the paper.

This work has been funded by IRGA (”Initiatives de Recherche à Grenoble Alpes”) project PaDeSoH (”Partial-differential-equation-based estimation of battery state of health”), in the framework of ”Investissement d’avenir” ANR-15-IDEX-02 French national research and innovation funding programme.

II. Single-particle modeling of a Li-ion cell

A battery cell consists basically in a superposition of porous positive and negative electrodes and the electrolyte, its main charging/discharging behavior being governed by intercalation (and desintercalation) of Li into the electrodes structure, as the cell is submitted to an electric current. It is widely agreed that this phenomenon, involving volumetric Li concentrations evolution within the electrodes, be modeled by a Fickian diffusion process, described by a set of parabolic partial-differential equations (PDEs) for every elementary particle (or grain) in the electrode. The mass transfer phenomena are here neglected. The cell terminal voltage is a function of the Li concentrations in each electrode [1]. SPM (Fig. 1) has been developed as an efficient way to predict Li concentrations' evolution and uses a single, equivalent spherical particle and a single PDE [2]. Next, subscripts "*p*" and "*n*" are used for positive and negative electrode, respectively.

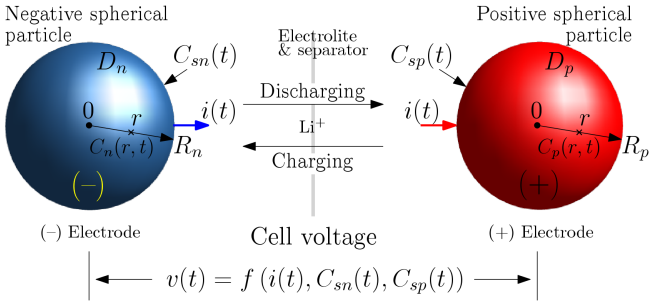

Fig. 1. SPM illustration, where each electrode is equivalent to a single spherical particle, of radius $R_{p/n}$.

1) Li concentrations within cell electrodes: are governed by a diffusion process written in the spherical coordinate:

$$\frac{\partial C_{p,n}}{\partial t}(r,t) = D_{p,n}\left[\frac{2}{r}\cdot\frac{\partial C_{p,n}}{\partial r}(r,t) + \frac{\partial^2 C_{p,n}}{\partial r^2}(r,t)\right], \quad (1)$$

where $C_{p,n}(r,t)$ denote the volumetric concentrations within the positive/negative sphere as functions of the radial coordinate r (along the sphere radius) and time t, and $D_{p,n}$ are the diffusivity coefficients in each of the electrodes, considered constant. Neumann boundary conditions are added to (1) in the particle's center and on its surface, respectively:

$$\begin{cases} \dfrac{\partial C_{p,n}}{\partial r}(0,t) = 0 \\ \dfrac{\partial C_{p,n}}{\partial r}(R_{p,n},t) = \dfrac{i(t)}{D_{p,n}F a_{p,n} A L_{p,n}}, \end{cases} \quad (2)$$

where F is Faraday's constant, $R_{p,n}$ are the particle radii, A is the cell area, $L_{p,n}$ are the electrode thicknesses, $a_{p,n}$ are the specific interfacial surface areas and $i(t)$ is the cell current, whose sign convention is $i(t) > 0$ when charging and $i(t) < 0$ when discharging. The cell voltage potential is determined by surface concentrations of both positive and negative electrodes, noted as $C_{sp}(t) = C_p(R_p,t)$ and $C_{sn}(t) = C_n(R_n,t)$, respectively, which are the solutions of (2) for each electrode.

In automotive applications, battery current is usually lower than 1C, when considering suitable vehicle autonomy. It is widely agreed that at these levels of cell current, Li^+ concentration values remain practically constant in the electrolyte and mass transport effects within it are negligible. Cell behavior can thus reasonably be described by (1) and (2) written for both particles, which give Li concentrations in both electrodes. Also, experimental tests on cells under EV-specific driving cycles (*e.g.*, [14]), showed sufficiently small cell temperature variations (within $\pm 1.5°C$), so that the temperature be reasonably considered constant within a discharge cycle.

2) Voltage of a cell: depends on current and on Li concentrations on particles' surfaces through a nonlinear algebraic relation describing the Butler-Volmer kinetics [3], [6]):

$$\begin{aligned} v_{bt}(t) = {} & \frac{RT}{\alpha_p F}\cdot \sinh^{-1}\left[\frac{i(t)}{2a_p A L_p i_0(C_{sp}(t))}\right] - \\ & - \frac{RT}{\alpha_n F}\cdot \sinh^{-1}\left[\frac{-i(t)}{2a_n A L_n i_0(C_{sn}(t))}\right] + R_f\cdot i(t) + \\ & + U_p(C_{sp}(t)) - U_n(C_{sn}(t)), \end{aligned} \quad (3)$$

where i_0 is the exchange current density for each electrode:

$$i_0(C_{sp,n}(t)) = k_{p,n}\sqrt{C_e^0\cdot C_{sp,n}(t)\,[C_{mxp,n} - C_{sp,n}(t)]} \quad (4)$$

and $\alpha_{p,n}$ are the anodic/cathodic transfer coefficients, $k_{p,n}$ are the reaction rates, $C_{mxp,n}$ are the maximum Li concentrations in solid phase, C_e^0 is the Li^+ concentration in electrolyte phase, R_f is the lumped current collector resistance, T is the cell temperature and R is the universal gas constant. Specific interfacial surface areas are defined as $a_{p,n} = \frac{3\varepsilon_{p,n}}{R_{p,n}}$, where volume fractions $\varepsilon_{p,n}$ are constant for a given electrode.

The first two right-side terms of (3) represent cell overpotentials (of the positive and the negative electrode, respectively), depending of both Li concentrations and the cell current and corresponding to a cumulative effect of a series resistance, which is variable with the Li concentrations on both particles' surfaces. Their inverse-hyperbolic-sine form corresponds to equal transfer coefficients, $\alpha_{p,n} = 0.5$, describing lithiation/delithiation reactions where a single electron per Li atom is exchanged. The third term denotes the overpotential due to the lumped internal resistance, R_f. $U_p(C_{sp}(t))$ and $U_n(C_{sn}(t))$ in (3) are the so-called equilibrium potentials, which are material-dependent functions of the amount of Li in the electrode (also called *degree of lithiation*), expressed by normalized surface concentrations in relation to their respective maximum values, $C_{mxp,n}$ – see Figs. 2 a) and b). Being characteristic of each type of electrode material, they are usually given in the literature either as look-up tables or as equations using transcendental functions [11]. Their difference gives the so-called cell open-circuit voltage: $V_{ocv}(t) = U_p(C_{sp}(t)) - U_n(C_{sn}(t))$.

3) The state-space model: of Li concentrations results from spatial derivative approximation *via* discretization of radial coordinate within each spherical particle.

Considering N internal discretization nodes within the sphere, radius $R_{p,n}$ is quantized in $(N+1)$ domains of $\Delta r_{p,n} = \frac{R_{p,n}}{(N+1)}$. As this discretization defines $(N+1)$ spherical shells of equal thickness, Li volumetric concentrations $C_{kp/n}(t)$ are defined within elementary volumes situated on the surface of each sphere having the index k. We note

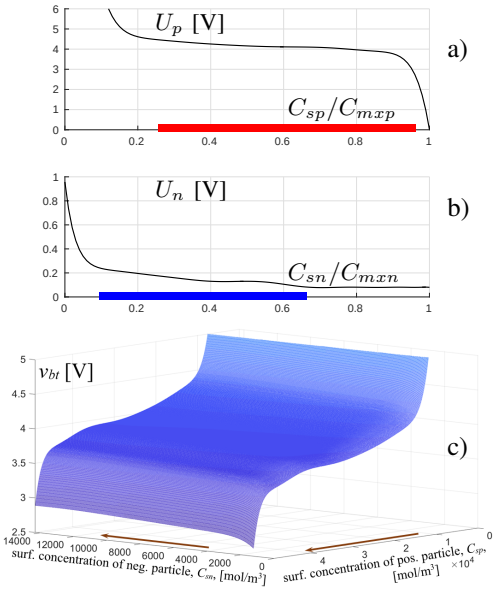

Fig. 2. Open-circuit potentials of a) positive and b) negative electrode *vs.* normalized surface concentrations [11]. c) Typical cell voltage variation *vs.* surface concentrations.

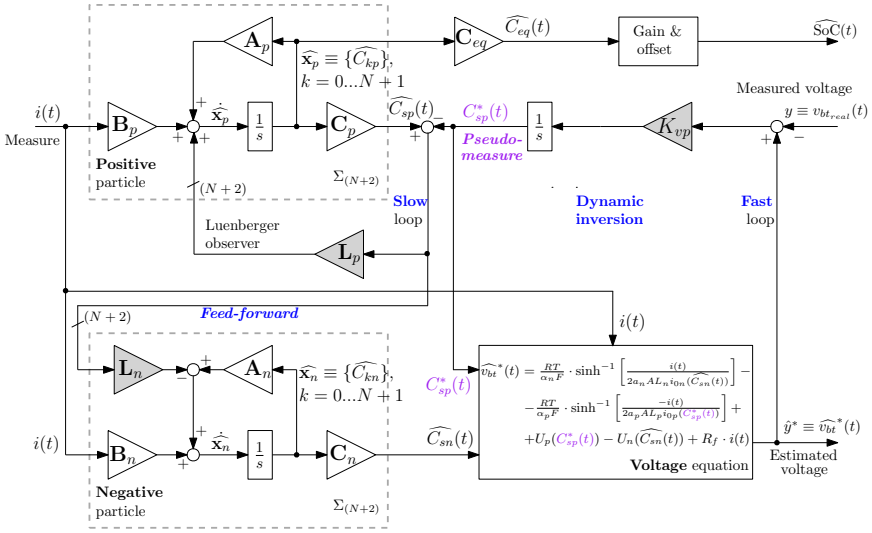

Fig. 3. SoC estimation with the proposed two-level observer, emphasizing the two-time-scale dynamics: a fast dynamic inversion and a slower Luenberger estimation, respectively. Only the positive particle is used for estimation, the negative one undertakes a feed-forward action. Gains to be selected are grayed.

the time constants $\tau_{p,n} = \frac{\Delta r_{p,n}^2}{D_{p,n}}$ and the gains $G_{p,n} = D_{p,n} F a_{p,n} A L_{p,n}$.

Furthermore, one uses the method of lines for approximating SPM PDE in (1) and Euler's forward difference method for the first spatial derivative approximation. However, in the second equation of (2) (*i.e.*, on the particle surface) backward differencing is used for derivative approximation. After some usual algebraic manipulations , a set of $(N+2)$ equations is obtained, which represents the complete model of Li concentrations' evolution within each particle:

$$\begin{cases} \dfrac{\mathrm{d}C_{0p,n}(t)}{\mathrm{d}t} = \dfrac{1}{\tau_{p,n}}\left[C_{1p,n}(t) - C_{0p,n}(t)\right] \\ \dfrac{\mathrm{d}C_{kp,n}(t)}{\mathrm{d}t} = \dfrac{1}{k\tau_{p,n}}\Big[(k+2)C_{(k+1)p,n}(t) - 2(k+1)C_{kp,n}(t) \\ \qquad\qquad + kC_{(k-1)p,n}(t)\Big], \quad k = 1, 2 \ldots N \\ \dfrac{\mathrm{d}C_{sp,n}(t)}{\mathrm{d}t} = \mp\dfrac{D_{p,n}(N+3)}{G_{p,n}R_{p,n}} i(t) \\ \qquad\qquad - \dfrac{1}{\tau_{p,n}}\left[C_{Np,n}(t) - C_{(N-1)p,n}(t)\right]. \end{cases} \tag{5}$$

The system state vector incorporates all Li concentrations in all spatial discretization points, including center of the generic spherical particle and its surface:

$\mathbf{x}_{p,n} = [C_{0p,n}(t)\ C_{1p,n}(t)\ \cdots\ C_{Np,n}(t)\ C_{sp,n}(t)\ ]^T$. With the cell current, $i(t)$, as input and the Li concentration on the surface of each of the particles, $C_{sp,n}(t) \equiv C_{(N+1)p,n}(t)$, as output the ODEs describing Li diffusion within the particle under the influence of the cell current lead to a (N+2)$^{\text{th}}$-order state-space model for each electrode:

$$\begin{cases} \dot{\mathbf{x}}_{p,n}(t) = \mathbf{A}_{p,n}\mathbf{x}_{p,n}(t) + \mathbf{B}_{p,n} i(t) \\ C_{sp,n}(t) = \mathbf{C}_{p,n}\mathbf{x}_{p,n}(t) \end{cases} \tag{6}$$

State-space matrices resulting from developing (5) for all discretization points k in the generic particle are given in (17) in the Appendix. Matrices $\mathbf{A}_{p,n}$ have both a zero eigenvalue – with all the other ones in the left-side complex plane – which shows an integration effect within the Li concentration buildup, corresponding to the charging/discharging process (or otherwise cell SoC evolution). The state matrices have a tri-diagonal structure and depend only on the time constants, $\tau_{p,n}$, and the number of spatial samples, N. The input matrices $\mathbf{B}_{p,n}$ have each a single, last-row, non-zero element, denoted next as the current gain, showing that the current acts directly only on the surface concentrations, $C_{sp,n}$. The two current gains, G_{ip} and G_{in}, respectively, have opposite signs, reflecting the opposite actions of current on the surface concentrations: for battery charging ($i(t) > 0$) that of positive particle diminishes and that of negative particle increases – and the opposite for discharging. These gains depend on the respective electrode geometry: surface, thickness and volume fraction:

$$G_{ip,n} = \mp\frac{D_{p,n}(N+3)}{G_{p,n}R_{p,n}} = \mp\frac{N+3}{3FA\varepsilon_{p,n}L_{p,n}}. \tag{7}$$

With $i(t) = 0$ in (6) – corresponding to what is called cell *relaxation* – an autonomous system is obtained, whose steady states are by definition the *equilibrium* Li *concentrations*, which thus depend on the initial concentrations just before zeroing the cell current. So the equilibrium concentrations directly reflect the cell SoC, namely, the one (just) before relaxation. Let us note surface concentrations at equilibrium at SoC=0 by $C_{p\mathbf{0}}$ and $C_{n\mathbf{0}}$ and at SoC=1 by $C_{p\mathbf{1}}$ and $C_{n\mathbf{1}}$, respectively. Starting from an initial given SoC – *i.e.*, from the corresponding initial concentrations – C_{sp} and C_{sn} are obtained by numerically integrating SPM equations (6)–(7) for both the positive and the negative particles. Then, the voltage results by using these concentrations and current $i(t)$ in (3).

Finally, the equilibrium concentration at a certain time t, noted as $C_{eq}(t)$, which directly represents the cell SoC, can be computed as the solution of the relaxation process that would begin at t if the current would be zeroed at t:

$$C_{eq}(t) = \mathbf{C}_{p,n} \cdot e^{(\mathbf{A}_{p,n} \cdot T_r)} \cdot \mathbf{x}_{p,n_{br}}, \quad (8)$$

where $\mathbf{C}_{p,n} = [0\ 0\ 0 \dots\ 0\ 1]$ (size of $N+2$), time value T_r is fixed, larger than the relaxation time, and $\mathbf{x}_{p,n_{br}}$ is the vector of concentrations just before relaxation. Note that $C_{eq}(t)$ can be approximated by a linear combination of either the concentrations $C_{pk}(t)$ or $C_{nk}(t)$:

$$C_{eq}(t) = \frac{6}{(N+1)(N+2)(2N+3)} \cdot \sum_{k=0}^{N+1} \left(k^2 C_{kp,n}(t)\right), \quad (9)$$

more accurate as the spatial sampling grid is finer (N larger).

III. Two-level SoC observer

The goal here is to recover the "true" cell SoC from an arbitrary one by using the available measured variables: current and voltage of the real cell. As the SoC is the linear combination (9) of internal Li concentrations of either the positive electrode or the negative one, the SoC estimation can be formulated as a state observation problem for the dynamical system with state equations (6) and output equation (3).

A. Proposed observer structure

The proposed observer structure exploits the specific model structure, detailed in Section II, and aims at employing a *divide-et-impera* approach. More specifically, it uses the fact that the high-order ($2(N+2)$) linear dynamical system giving the surface Li concentrations in both particles feeds a nonlinear voltage function as output. The two types of complexity – due to nonlinearity and to the high-order modeling, respectively – are thus dealt with separately, as shown in Fig. 3.

First, a dynamic inversion scheme is used to get the surface concentration of that of the particles exhibiting the faster dynamics – here, the positive one, as $\tau_p < \tau_n$ – which represents one of the inputs of the nonlinear voltage function. This is done by integrating the error between real cell voltage, $v_{bt_{real}}(t)$, and model output voltage, $v_{bt}(t)$. In this way, a pseudo-measure of surface Li concentration for the positive particle, $C^*_{sp}(t)$, is obtained. It serves as a reference for the second level of estimation.

At the second (lower) estimation level, estimates of all internal Li concentrations are obtained, by means of a Luenberger observer [15], which minimizes the error between the model-computed surface Li concentration, $\widehat{C_{sp}}(t)$, and its pseudo-measure, $C^*_{sp}(t)$, provided by the first (upper) estimation level.

The first-level dynamic inversion should be significantly faster *vs.* the second-level linear observation loop, which is achieved by using a suitably large integrator gain, K_v. A certain slow dynamics for the estimated states (concentrations at various coordinates in positive and negative spheres) can then be imposed by pole placement, as $(\mathbf{A}_p, \mathbf{C}_p)$ matrix pair is detectable, resulting in the second-level observer vector gain, $\mathbf{L}_p$ – see the justification below.

This results in the second level observer gains $\mathbf{L}_p$ and $\mathbf{L}_n$. Note that, from physical interpretation, $\mathbf{L}_p$ and $\mathbf{L}_n$ should also be related with each other: if indeed the estimation for the positive sphere relies on a gain $\mathbf{L}_p$ (related to the $(\mathbf{A}_p, \mathbf{C}_p)$ pair), the estimates of concentrations in the negative, slower particle, $\widehat{C_{sn}}(t)$, are in fact adjusted *via* a feed-forward action, by means of a vector gain $\mathbf{L}_n$, which should be consistent with the conservation of total Li species.

This is because observer implementation supposes an alteration of the estimated states' derivatives in the positive particle, which can be viewed as an additional current-like action on all the surfaces $k = 0, 1, ...N+1$. An equivalent action should thus be applied for the negative particle, by virtue of the above-mentioned conservation law. So the same error, *i.e.*, that of surface concentration of positive electrode, $\widehat{C_{sp}} - C^*_{sp}$, will also drive estimation for the negative one, to ensure that its internal Li concentrations are also correctly estimated. Therefore, the cell SoC estimate can further be computed based on either $\widehat{C_{kp}}$ or $\widehat{C_{kn}}$, $k = 1, 2...N+2$.

As it is also emphasized by the convergence proof in the next subsection, III-B, rapidity of dynamic inversion is crucial to initiate the estimation convergence process, as in this way a pseudo-measure of the surface concentration, even if approximate in a first place, is made available for the second estimation level. At this latter level, the effective state estimation takes place: first for the positive particle *via* Luenberger observer and then for the negative particle by means of feed-forward correction. This iterative process ensures minimization of the voltage error and ultimately a reliable SoC estimation through the estimated equilibrium concentration, $\widehat{C_{eq}}(t)$, computed according to (9) based on positive electrode's internal Li concentrations, $\widehat{C_{kp}}$. Matrix $\mathbf{C}_{eq}$ in Fig. 3 results from (9).

B. Convergence proof and observer design guidelines

Let us resume the state-space model (6) of both electrodes' internal concentrations and cell voltage (3) as output, $y \equiv v_{bt}$:

$$\begin{aligned} \dot{\mathbf{x}_p} &= \mathbf{A}_p \mathbf{x}_p + \mathbf{B}_p i \\ \dot{\mathbf{x}_n} &= \mathbf{A}_n \mathbf{x}_n + \mathbf{B}_n i \\ y &= h_p(C_{sp}, i) + h_n(C_{sn}, i) + R_f i \end{aligned} \quad (10)$$

with surface concentrations given by $C_{sp} = \mathbf{C}_p \mathbf{x}_p$ and $C_{sn} = \mathbf{C}_n \mathbf{x}_n$, respectively, where matrices $\mathbf{A}_p, \mathbf{A}_n, \mathbf{B}_p, \mathbf{B}_n, \mathbf{C}_p, \mathbf{C}_n$ are given in the Appendix and functions h_p, h_n can be identified in (3). According to the overall scheme in Fig. 3, the proposed observer takes the following form:

$$\begin{aligned} \dot{C}^*_{sp} &= K_v(\hat{y}^* - y) \\ \dot{\widehat{\mathbf{x}_p}} &= \mathbf{A}_p \widehat{\mathbf{x}_p} + \mathbf{B}_p i + \mathbf{L}_p(\widehat{C_{sp}} - C^*_{sp}) \\ \dot{\widehat{\mathbf{x}_n}} &= \mathbf{A}_n \widehat{\mathbf{x}_n} + \mathbf{B}_n i - \mathbf{L}_n(\widehat{C_{sp}} - C^*_{sp}) \\ \hat{y}^* &= h_p(C^*_{sp}, i) + h_n(\widehat{C_{sn}}, i) + R_f i \end{aligned} \quad (11)$$

for appropriate gains $\mathbf{L}_p, \mathbf{L}_n, K_v$.

Notice first that we will use the following properties on h_p, h_n, which hold for some constants $\alpha > 0$ and $\beta > 0$ in the considered operating conditions, as suggested by Fig. 2 c), showing some typical variation of a battery voltage with electrodes' surface concentrations:

$$
\begin{array}{ll}
(P1) & \dfrac{\partial h_p}{\partial C_{sp}}(C_{sp}, i) \leq -\alpha \\
(P2) & \dfrac{\partial h_n}{\partial C_{sn}}(C_{sn}, i) \simeq -\beta \dfrac{\partial h_p}{\partial C_{sp}}(C_{sp}, i),
\end{array}
\tag{12}
$$

together with boundedness of $\dot{C}_{sp}$. Note also that, in practice, an estimate of β is given by $-\frac{\mathbf{C}_p\mathbf{B}_p}{\mathbf{C}_n\mathbf{B}_n} = -\frac{G_{ip}}{G_{in}}$, hence β can be used in the design (while no knowledge on α is needed).

In addition, from the forms of $\mathbf{A}_p, \mathbf{A}_n, \mathbf{C}_p, \mathbf{C}_n$ one can check the following property:

$(P3)$ $(\mathbf{A}_{pn}, \mathbf{C}_{pn})$ matrix pair is detectable,

$$\text{where } \mathbf{A}_{pn} := \begin{pmatrix} \mathbf{A}_p & 0 \\ 0 & \mathbf{A}_n \end{pmatrix}, \ \mathbf{C}_{pn} := \begin{pmatrix} \mathbf{C}_p & -\beta\mathbf{C}_n \end{pmatrix}$$

This follows from the fact that both $\mathbf{A}_p$ and $\mathbf{A}_n$ have all their eigenvalues with strictly negative real parts, except one at 0. Hence, $\mathbf{A}_{pn}$ has only two unstable eigenvalues, both equal to zero. It can easily be checked that the related eigenvectors are:

$$v_1 = \begin{pmatrix} 1_{1\times(N+2)} & 0_{1\times(N+2)} \end{pmatrix}^T, v_2 = \begin{pmatrix} 0_{1\times(N+2)} & 1_{1\times(N+2)} \end{pmatrix}^T$$

where $a_{1\times(N+2)}$ stands for a row vector of $N+2$ components, all equal to a ($N+2$ being the dimension of both $\mathbf{x}_p$ and $\mathbf{x}_n$). It is also obvious that $C_{pn}v_1 \neq 0$ and $C_{pn}v_2 \neq 0$, meaning that the zero eigenvalues of $\mathbf{A}_{pn}$ are observable.

Let us now set $h_{pd} := \dfrac{\partial h_p}{\partial C_{sp}}$ and $h_{nd} := \dfrac{\partial h_n}{\partial C_{sn}}$ and define estimation errors $\mathbf{e}_p := \widehat{\mathbf{x}_p} - \mathbf{x}_p$, $\mathbf{e}_n := \widehat{\mathbf{x}_n} - \mathbf{x}_n$ and $e^*_{sp} := C^*_{sp} - C_{sp}$. Then, considering a first order approximation for dynamics of e^*_{sp}, we get:

$$\dot{e}^*_{sp} \simeq K_v h_{pd} e^*_{sp} + K_v h_{nd} \mathbf{C}_n \mathbf{e}_n - \dot{C}_{sp} \tag{13}$$

On the other hand, we can derive from (10)–(11) the following error equations:

$$
\begin{array}{rcl}
\dot{\mathbf{e}_p} & = & (\mathbf{A}_p + \mathbf{L}_p\mathbf{C}_p)\mathbf{e}_p - \mathbf{L}_p e^*_{sp} \\
\dot{\mathbf{e}_n} & = & \mathbf{A}_n\mathbf{e}_n - \mathbf{L}_n\mathbf{C}_p\mathbf{e}_p + \mathbf{L}_n e^*_{sp} \\
& = & (\mathbf{A}_n - \frac{h_{nd}}{h_{pd}}\mathbf{L}_n\mathbf{C}_n)\mathbf{e}_n + \mathbf{L}_n(e^*_{sp} + \frac{h_{nd}}{h_{pd}}\mathbf{C}_n\mathbf{e}_n) \\
& & -\mathbf{L}_n\mathbf{C}_p\mathbf{e}_p
\end{array}
\tag{14}
$$

Notice here that, by using property $(P2)$, we have that $\mathbf{e}_n$ is driven by $\mathbf{A}_n + \beta\mathbf{L}_n\mathbf{C}_n$ (while $\mathbf{e}_p$ is driven by $\mathbf{A}_p + \mathbf{L}_p\mathbf{C}_p$).

Next, assuming that K_v is chosen large enough, we clearly obtain that (13)–(14) defines a two-time-scale system, whose boundary layer takes the following form:

$$\dot{\xi} = h_{pd} \cdot \xi, \tag{15}$$

for which 0 is clearly uniformly exponentially stable by property $(P1)$. Then the related reduced system becomes:

$$
\begin{array}{rcl}
\dot{\mathbf{e}_p} & = & (\mathbf{A}_p + \mathbf{L}_p\mathbf{C}_p)\mathbf{e}_p - \beta\mathbf{L}_p\mathbf{C}_n\mathbf{e}_n \\
\dot{\mathbf{e}_n} & = & (\mathbf{A}_n + \beta\mathbf{L}_n\mathbf{C}_n)\mathbf{e}_n - \mathbf{L}_n\mathbf{C}_p\mathbf{e}_p
\end{array}
\tag{16}
$$

Now, we can use property $(P3)$ to design $\mathbf{L}_{pn}$ so that $\mathbf{A}_{pn} + \mathbf{L}_{pn}\mathbf{C}_{pn}$ to be Hurwitz, and we thus just need to select $\mathbf{L}_p$ and $\mathbf{L}_n$ with $\begin{pmatrix} \mathbf{L}_p \\ -\mathbf{L}_n \end{pmatrix} = \mathbf{L}_{pn}$ such that to ensure the origin of error system (16) being exponentially stable. Finally, according to Tikhonov theorem [16], the solution of error system (13)–(14) approaches 0 with an accuracy driven by $\frac{1}{K_v}$.

IV. Cell SoC estimation results in an electric vehicle use case

This section presents SoC estimation performance in an electric vehicle (EV) use case, *i.e.*, for battery cells being submitted to EV-specific driving cycles. Here, a current profile derived from the Worldwide Harmonized Light Vehicles Test Procedure (WLTP) [14] was used in both MATLAB® /Simulink® simulations and real-world tests; its negative-average variation in Fig. 4 obviously reflects a battery discharging process. Real-data validation was based on voltage measures provided by a BCS-800-series battery cycler [17].

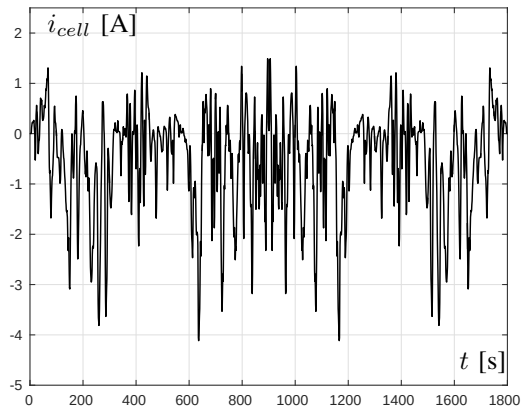

Fig. 4. WLTP-like current profile used for SoC estimation validation.

A. Numerical simulation results

Here, the goal is to force the estimation performance limits – in absence of any noise, parameter uncertainty and unmodelled dynamics – in order to illustrate that design parameters – especially the dynamic inversion gain, K_v – are adjustable in a large range, thus confirming the formal findings in Subsection III-B. SPM parameters of the battery used in simulations are given in Table I in the Appendix. In the simulation scenario convergence of the proposed observer is checked when the state-space SPM model and the observer, both excited with the WLTP-like current profile in Fig. 4, repeated nine times, have some initial states corresponding to very different SoC values. A case where $\text{SoC}_{obs0} = 0.55$ is smaller than that of the model, $\text{SoC}_{model0} \approx 0.9$, was considered. A large gain, $K_v = 35000$, was used to enable very fast recovering of the "real" SoC, while the Luenberger observer gain, $\mathbf{L}_p$, is a constant vector filled with -6 and $\mathbf{L}_n$ vector gain is filled with -2.667. Table I in the Appendix contains parameters' values resulting from previous SPM calibration against tests on real cells, *e.g.*, according to the method proposed in [18].

Fig. 5 a) shows the estimated SoC *vs.* the SoC computed by Coulomb counting (integration of current $i(t)$) and the model-computed one, denoted as the "real" one. The SoC recovering time is very small, less than 10 s – see the zoom around time 0. The error between the three SoC signals is detailed in zoom 1. Total evolution of estimation error can be seen in Fig. 5 b), the maximum error being less than 2% (see zoom 2).

Voltage variations in Fig. 6 a) and zoom 1 suggest that the model-given (or "real") voltage ($v_{bt_{real}}$ in Fig. 3) is very

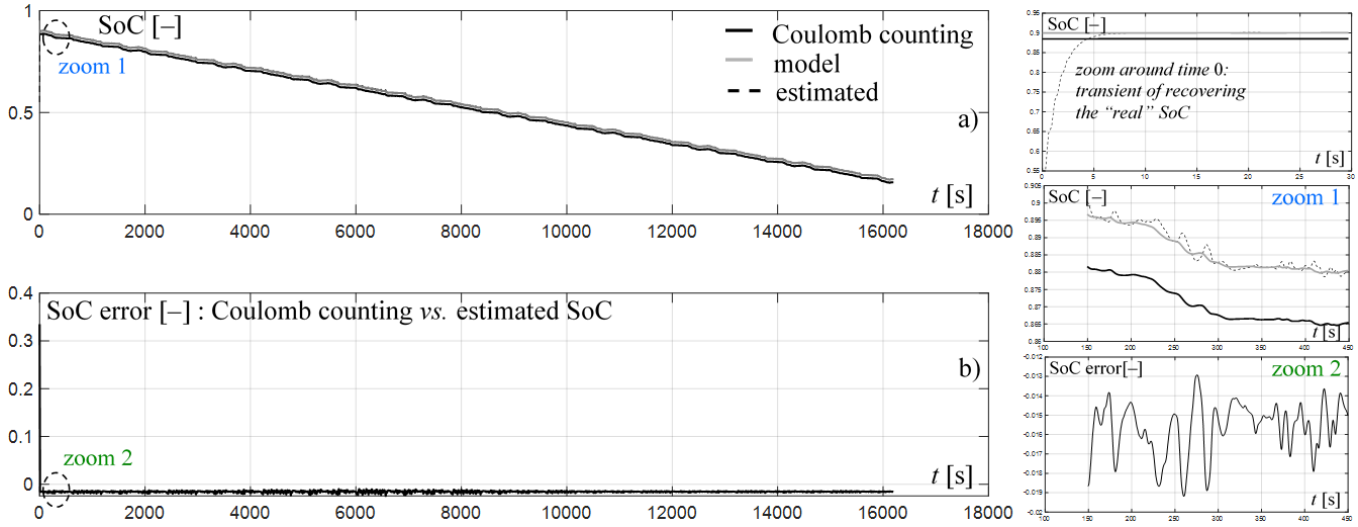

Fig. 5. SoC evolution during an almost complete battery discharge and associated zoomed pictures: a) model and estimated values *vs.* Coulomb counting value taken as baseline; b) SoC estimation error.

accurately tracked by the one computed based on estimated surface concentrations ($\widehat{v_{bt}}^*$ in Fig. 3). Figs. 6 b) and c) show evolutions of positive and negative surface concentrations, C_{sp} and C_{sn}, respectively, for both the model and the observer. Estimation accuracies are shown in zooms 2 and 3, respectively.

B. Estimation results on real data

The real-data estimation scenario was carried out for a battery submitted to the same excitation current as in simulation, this time on a BCS-800-series battery cycler. In this case, calibration of SPM parameters indicated that it is the *negative* electrode's dynamic which is faster – *i.e.*, $\tau_n \leq \tau_p$ – so the estimation was performed on it, with the upper-level dynamic inversion providing this time a pseudo-measure of the *negative* particle's surface concentration, C^*_{sn}, send as reference for the second estimation level. Here also, the battery and the observer have some initial states corresponding to different SoC values, namely $\text{SoC}_{obs0} = 0.55$ was smaller than the real $SoC = 0.885$, as given by Coulomb counting.

Real-data-based estimation has some particularities, as follows. Low-pass filtering was necessary to denoise the voltage error, $\widehat{v_{bt}}^*(t) - v_{bt_{real}}(t)$. In order to enable fast recovering of the real SoC, the dynamic inversion gain was rendered adaptive in the sense of decreasing with the voltage error squared: $K_v = K_{v_{nom}}[\widehat{v_{bt}}^*(t) - v_{bt_{real}}(t)]^2$, with $K_{v_{nom}} = 850$. Lower-level estimation vector gains, $\mathbf{L}_p$ and $\mathbf{L}_n$, exchange their roles, with the Luenberger observer gain, $\mathbf{L}_n$, being a constant vector filled with -6.25 and $\mathbf{L}_p$ being filled with -14.0625.

Fig. 7 a) shows the estimated SoC *vs.* the SoC computed by Coulomb counting (integration of current $i(t)$), which was considered as the true SoC value. The SoC is here recovered in about 300 s. Fig. 7 b) shows the total evolution of estimation error and the associated zoom indicates a maximum error being less than 3.5%. Voltage variations in Fig. 8, along with a zoomed part of the plot, suggest good tracking of the measured values, $v_{bt_{real}}$ by the one computed based on estimated surface concentrations, $\widehat{v_{bt}}^*$.

Figs. 9 a) and b) show evolutions of all estimated internal Li concentrations inside the positive and the negative electrode, respectively. In both cases, surface concentrations are the mostly variable, as they are directly influenced by the input current action. Note the significantly larger dispersion of positive particle's concentrations, C_{kp}, in relation to the negative particle's ones, C_{kn}, and also the spatial filtering effect resulting in the center concentrations, C_{0p} and C_{0n}, respectively, having the smoothest variations.

V. Conclusion

This paper has investigated the problem of lithium-ion battery SoC estimation starting from an electrochemical model that describes the internal diffusion phenomena governing the charging/discharging process. Thus, the parabolic-partial-differential-equation Single Particle Model (SPM), in which each electrode is represented as a single spherical particle, has been adopted. It has next been approximated by a linear finite-dimensional state-space model – namey, by 1D spatial discretization of each particle (electrode), from its center to its surface – whose states are the Li volumetric internal concentrations at each discretization point. Further, the temperature being supposed invariant, the equilibrium concentration – a direct image of battery SoC – can be estimated as as a linear combination of these concentrations – out of which the surface ones play a special role, as the measurable battery voltage depends on nonlinearly – provided that SPM parameters had previously been identified, *e.g.*, by model calibration against measured data.

In this paper a two-level hierarchical observer is proposed for SoC estimation, within an approach consistent with an engineering practice viewpoint aiming at simplicity of tuning, implementation and integration as a BMS advanced function. Thus, the two dynamically-separated estimation levels reflect the multi-time-scale nature of battery internal phenomena: a fast level achieving a dynamic inversion, aimed at retrieving surface Li concentrations from the battery measured voltage, and a slow level, in which the internal Li concentrations

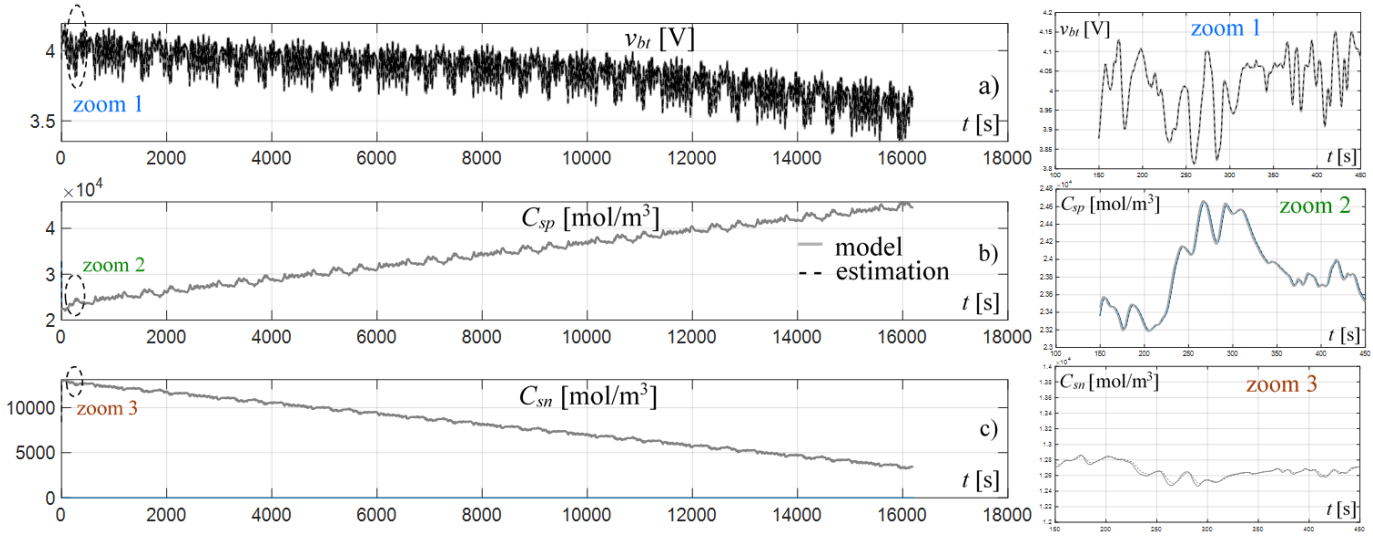

Fig. 6. Evolution of cell voltage and surface concentrations and associated zoomed pictures: a) model *vs.* estimated voltage; b) surface concentration of positive particle: model, C_{sp}, and estimated, $\widehat{C_{sp}}$, almost perfectly equal to the reference (pseudo-measure) provided by the dynamic-inversion loop, C^*_{sp}; c) surface concentration of negative particle: model, C_{sn}, and estimated, $\widehat{C_{sn}}$.

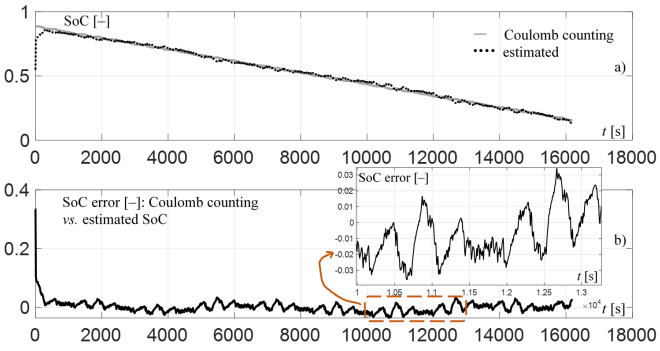

Fig. 7. SoC evolution as the battery is submitted to the same current $i(t)$ as in simulation and observer is based on real measured voltage values: a) estimated value *vs.* Coulomb counting value taken as baseline; b) SoC estimation error and zoom indicating its maximum at around 3.5%.

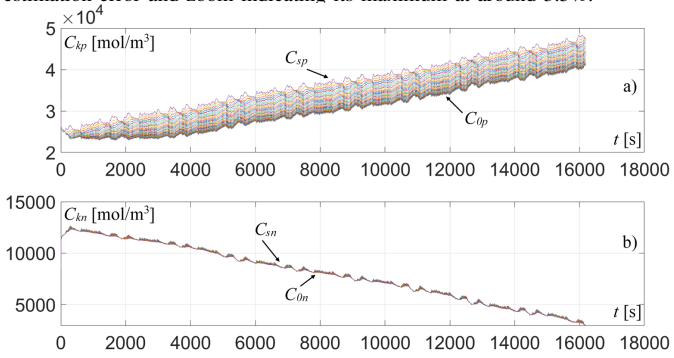

Fig. 9. Totality of the $N + 2 = 32$ real-voltage-based estimated internal Li concentrations, of the a) positive particle and b) negative one.

are estimated by using a classical Luenberger observer. As illustrated by numerical simulations and also by using real voltage measures (relevant to electric-vehicle (EV) use cases), this structure is easy to tune and allows avoiding frequent convergence issues occurring in the case of a global, one-level estimation and which are partly due to an intrinsically ill numerical conditioning of the linear approximated model.

It has been proven that SoC estimation accuracy and rapidity

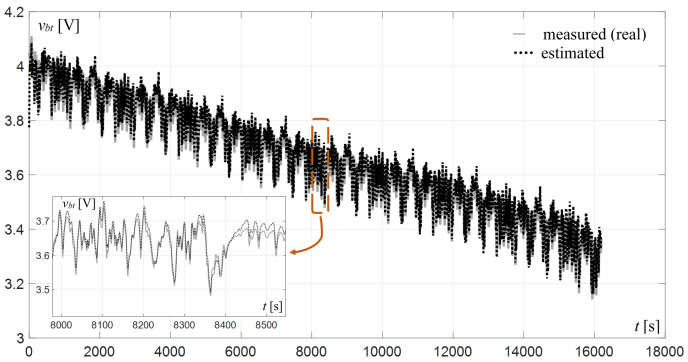

Fig. 8. Evolution of the cell voltage: measured, $v_{bt_{real}}(t)$, *vs.* estimated, $\widehat{v_{bt}}^*(t)$ – and zoomed plot in between 8000 s and 8500 s.

mainly depends on the upper-level gain, implementing the dynamic inversion by integrating the error between the real voltage and the estimated one. Thus, the faster this level obtains a so-called pseudo-measure of surface concentration, the better is for the lower level, which receives this pseudo-measure as a reference and, at its turn, minimizes the error between reference and estimation. As SoC estimation can be equivalently based on either of the electrode's surface concentration, the observer will act on the one with the faster concentrations' dynamics, according to the state-space SPM. This *divide-et-impera* approach allows the two types of complexity – due to nonlinearity and to the high-order modeling, respectively – being dealt with separately. Validation on real data issued from battery cycling under input current profiles corresponding to standard EV driving cycle scenarios has shown estimation errors – in relation to baseline SoC estimation by Coulomb counting – less than 3.5%, which suggests very good performance.

Two main research directions may further be envisaged. One of them is to deepen the study of formal properties of the proposed observer towards possible generalizations to a

larger class of systems. A second direction is to investigate both practical implementation issues of the proposed SoC observer – in terms of computational burden *vs.* time criticality, robustness to various parameter uncertainties and possibly unmodelled dynamics – and its use as a software sensor for battery tests in various states of health (SoH), to emphasize the inter-relation between SoC and SoH, and possibly with other battery operation key variables.

ACKNOWLEDGMENT

The authors would like to thank Dr. Céline Decaux and Dr. Rakesh Khatokar Amarnath from LEPMI for their effective support during the experimental tests on Li-ion cells.

REFERENCES

[1] N. A. Chaturvedi, R. Klein, J. Christensen, J. Ahmed, and A. Kojić, "Algorithms for advanced Battery Management Systems," IEEE Control Systems Magazine, vol. 30, no. 3, pp. 49–68, June 2010.

[2] D. Di Domenico, A. Stefanopoulou, and G. Fiengo, "Lithium-ion battery state of charge and critical surface charge estimation using an electrochemical model-based extended Kalman filter," Journal of Dynamic Systems, Measurement, and Control, 132(6), 061302, November 2010.

[3] R. Klein, N. A. Chaturvedi, J. Christensen, J. Ahmed, R. Findeisen, and A. Kojić, "Electrochemical model based observer design for a lithium-ion battery," IEEE Trans. Contr. Syst. Technol., vol. 21, no. 2, pp. 289–301, January 2012.

[4] S. J. Moura, F. B. Argomedo, R. Klein, A. Mirtabatabaei, and M. Krstić, "Battery state estimation for a Single Particle Model with electrolyte dynamics," IEEE Trans. Contr. Syst. Technol., vol. 25, no. 2, pp. 453–468, March 2017.

[5] D. Zhang, B. N. Popov, and R. E. White, "Modeling lithium intercalation of a single spinel particle under potentiodynamic control," Journal of the Electrochemical Society, 147(3), 831, March 2000.

[6] S. J. Moura, M Krstić, and N. A. Chaturvedi, "Adaptive PDE observer for battery SOC/SOH estimation," in Procs. of Dynamic Systems and Control Conference, American Society of Mechanical Engineers, vol. 45295, pp. 101–110, October 2012.

[7] P. Blondel, R. Postoyan, S. Raël, S. Benjamin, and Ph. Desprez, "Nonlinear circle-criterion observer design for an electrochemical battery model," IEEE Trans. Contr. Syst. Technol., vol. 27, no. 2, pp. 889–897, March 2019.

[8] E. Petri, T. Reynaudo, R. Postoyan, D. Astolfi, D. Nešić, and S. Raël, "State estimation of an electrochemical lithium-ion battery model: improved observer performance by hybrid redesign," in Procs. of 2023 European Control Conf. (ECC 2023), June 13-16 2023, Bucharest, Romania.

[9] A. Allam and S. Onori, "Online capacity estimation for lithium-ion battery cells via an electrochemical model-based adaptive interconnected observer," IEEE Trans. Contr. Syst. Technol., vol. 29, no. 4, pp. 1636–1651, July 2021.

[10] A. M. Bizeray, J. H. Kim, S. R. Duncan, and D. A. Howey, "Identifiability and parameter estimation of the single particle lithium-ion battery model," IEEE Trans. Contr. Syst. Technol., 27(5), pp. 1862–1877, 2018.

[11] W. Li, D. Cao, D. Jöst, F. Ringbeck, M. Kuipers, F. Frie, and D. U. Sauer, "Parameter sensitivity analysis of electrochemical model-based battery management systems for lithium-ion batteries," Applied Energy, 269, 115104, July 2020.

[12] X. Han, M. Ouyang, L. Lu, and J. Li, "Simplification of physics-based electrochemical model for lithium ion battery on electric vehicle. Part I: Diffusion simplification and Single Particle Model,", Journal of Power Sources, 278, pp. 802–813, 2015.

[13] L. Li, Y. Ren, K. O'Regan, U. R. Koleti, E. Kendrick, W. D. Widanage, and J. Marco, "Lithium-ion battery cathode and anode potential observer based on reduced-order electrochemical Single Particle Model," Journal of Energy Storage, 44, 103324, 2021.

[14] ***, "Worldwide Harmonized Light Vehicles Test Cycle – WLTP3," https://dieselnet.com/standards/cycles/wltp.php#cycles, February 2024.

[15] D. Luenberger, "An introduction to observers," IEEE Transactions on Automatic Control, vol. AC-16, no. 6, pp. 596–602, December 1971.

[16] H. Khalil, Nonlinear Systems, 3rd Ed., Prentice Hall, 2002.

[17] ***, "BioLogic ultra-precision battery cycler," https://www.biologic.net/products/bcs-800/, February 2024.

[18] I. Munteanu, A. I. Bratcu, P.-X. Thivel, Y. Bultel, D. Georges, and C. Decaux, "Single-Particle Model of Li-ion battery – Model calibration and validation against real data in an electric vehicular application", submitted to the 12th IFAC Symposium on Control of Power and Energy Systems (CPES 2024), July 10–12, Rabat, Morocco.

APPENDIX

TABLE I

SPM PARAMETER VALUES USED IN NUMERICAL SIMULATION.

Symbol	Signification	Value
Common parameters		
N [-]	No. of discretization points	30
A [m2]	Electrode area	0.1
C_0^e[mol/m3]	Electrolyte Li^+ concentration	1000
R_f [Ω]	Internal ohmic resistance	0.020
T [K]	Cell temperature	298.15
R [J/mol/K]	Universal gas constant	8.31446
F[C/mol]	Faraday constant	96487
Negative particle		
D_n [m2/s]	Diffusivity in graphite	$3.9 \cdot 10^{-14}$
ε_n	Electrode volume fraction	0.75
α_n	Reaction transfer coefficient	0.5
C_{mxn} [mol/m3]	Maximum Li^+ concentration	30555
L_n [m]	Electrode thickness	$83 \cdot 10^{-6}$
R_n [m]	Particle radius	$20 \cdot 10^{-6}$
a_n [m2/m3]	Specific interfacial surface area	$1.125 \cdot 10^5$
k_n [m4/mol s]	Electrode reaction rate	$2 \cdot 10^{-6}$
τ_n [s]	Time constant	10.67
G_{in} [mol/m3/s/A]	Current gain	0.555
Positive particle		
D_p [m2/s]	Diffusivity in AM	$1.92 \cdot 10^{-16}$
ε_p	Electrode volume fraction	0.5
α_p	Reaction transfer coefficient	0.5
C_{mxp} [mol/m3]	Maximum Li^+ concentration	51555
L_p [m]	Electrode thickness	$75 \cdot 10^{-6}$
R_p [m]	Particle radius	$0.75 \cdot 10^{-6}$
a_p [m2/m3]	Specific interfacial surface area	$2 \cdot 10^6$
k_p [m4/mol s]	Electrode reaction rate	$1.25 \cdot 10^{-7}$
τ_p [s]	Time constant	3.05
G_{ip} [mol/m3/s/A]	Current gain	-0.921

$$\mathbf{A}_{p,n} = \begin{bmatrix} -\frac{1}{\tau_{p,n}} & \frac{1}{\tau_{p,n}} & 0 & 0 & 0 & 0 & 0 & 0 \\ \frac{1}{\tau_{p,n}} & -\frac{2(1+1)}{1\cdot\tau_{p,n}} & \frac{1+2}{1\cdot\tau_{p,n}} & 0 & 0 & 0 & 0 & 0 \\ 0 & \cdots & \cdots & \cdots & \cdots & \cdots & 0 & 0 \\ 0 & \cdots & \frac{1}{\tau_{p,n}} & -\frac{2k}{(k-1)\tau_{p,n}} & \frac{k+1}{(k-1)\tau_{p,n}} & 0 & \cdots & 0 \\ 0 & 0 & \cdots & \cdots & \cdots & \cdots & 0 & 0 \\ 0 & 0 & 0 & 0 & \frac{1}{\tau_{p,n}} & -\frac{2N}{(N-1)\tau_{p,n}} & \frac{N+1}{(N-1)\tau_{p,n}} & 0 \\ 0 & 0 & 0 & 0 & 0 & \frac{1}{\tau_{p,n}} & -\frac{2(N+1)}{N\tau_{p,n}} & \frac{N+2}{N\tau_{p,n}} \\ 0 & 0 & 0 & 0 & 0 & \frac{1}{\tau_{p,n}} & -\frac{1}{\tau_{p,n}} & 0 \end{bmatrix}, \quad \mathbf{B}_{p,n} = \begin{bmatrix} 0 \\ 0 \\ 0 \\ \vdots \\ 0 \\ 0 \\ G_{ip,n} \end{bmatrix}, \tag{17}$$

$$\mathbf{C}_{p,n} = \begin{bmatrix} 0 & 0 & 0 & \cdots & 0 & 0 & 1 \end{bmatrix}.$$